Contents lists available at ScienceDirect

Physics and Imaging in Radiation Oncology
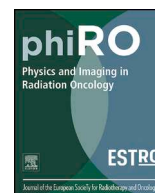
Original Research Article

A treatment planning study of combined carbon ion-beam plus photon intensity-modulated radiotherapy

Christopher Schuppert[a,*], Angela Paul[a], Simeon Nill[b], Andrea Schwahofer[c], Jürgen Debus[a], Florian Sterzing[a]

[a] *Department of Radiation Oncology and Radiation Therapy, University Hospital Heidelberg, Im Neuenheimer Feld 400, 69120 Heidelberg, Germany*
[b] *Joint Department of Physics, The Institute of Cancer Research and The Royal Marsden NHS Foundation Trust, London SM2 5PT, United Kingdom*
[c] *Department of Medical Physics in Radiation Oncology, German Cancer Research Center, Im Neuenheimer Feld 280, 69120 Heidelberg, Germany*

A B S T R A C T

Background and purpose: Combined photon intensity-modulated radiotherapy (IMRT) and sequential dose-escalated carbon ion beam therapy (IBT) is a technically advanced treatment option for head and neck malignancies. We proposed and evaluated an integrated planning strategy as opposed to an established and largely separated planning workflow.

Materials and methods: Ten patients with representative malignancies of the head and neck region underwent combined carbon-photon radiotherapy (RT) in our facilities. Clinical plans were created according to the separated workflow with independent optimization stages for both modalities. Experimental plans incorporated the existing carbon IBT dose distribution into the optimization stage of a step-and-shoot photon IMRT (bias dose planning).

Results: Cumulative dose distributions showed statistically significant differences between the two planning strategies and were predominantly in favor of the integrated approach. As such, target irradiation was generally maintained or even improved in a subset of metrics, while normal tissue sparing was widely enhanced; for instance, in the ipsilateral temporal lobe with median D_{mean} of -16% ($p < 0.001$). Maximum doses $D_{1\%}$ (with adjustment for different fractionation) fell below thresholds for toxicity risk in a minority of instances, where they were previously exceeded. Integral dose did not differ significantly.

Conclusions: Our findings indicate that combination planning of carbon-photon RT for head and neck malignancies may benefit from a proposed bias dose method, yielding favorable dose distribution characteristics and a streamlined planning workflow with fewer plan revisions. Further research is necessary to validate these observations in terms of robustness and their potential for higher tumor control.

1. Introduction

Head and neck malignancies comprise a heterogeneous group of epithelial cancers, predominantly located in the orbital region as well as the upper aerodigestive tract. With an estimated global incidence of 710.000 cases and 360.000 deaths every year (thyroid cancer excluded), they represent a critical cause of cancer-related mortality [1].

Treatment concepts differ considerably depending on tumor site and stage, and may require multidisciplinary collaboration between surgeons, medical oncologists, and radiation oncologists. Radiotherapy (RT) is a frequent option for neoadjuvant, adjuvant, or definitive treatment and continues to be the subject of extensive research. In addition to traditional RT modalities, heavy ion-beam radiotherapy

(IBT) has recently been brought to clinical maturity. A small number of specialized institutions have since investigated the potential of mixed-beam radiotherapy regimens that conjoin photon intensity-modulated radiotherapy (IMRT) and a sequential dose-escalated heavy ion boost using the C12 isotope [2–5]. Compared to a unimodal carbon treatment, combined carbon-photon RT reduces sensitivity to geometrical variances in the presence of steep dose gradients, either due to patient misalignment or interfractional changes in anatomy, thereby securing treatment effectiveness. At the same time, it leverages the superior capabilities of carbon over photon irradiation in the sparing of organs at risk (OARs). The studies above have positively attested to these complementary characteristics, and also asserted their clinical relevance in the form of higher locoregional control (LC) rates than those of

---

* Corresponding author.
  E-mail address: christopher.schuppert@med.uni-heidelberg.de (C. Schuppert).

unimodal photon regimens: *Schulz-Ertner et al.*, for instance, found that for locally advanced ACCs, a combination of carbon IBT and stereotactic photon RT (applied as fractionated stereotactic radiotherapy (FSRT) or IMRT) showed higher LC rates after four years than stereotactic photon RT alone (78% vs. 25%, although not statistically significant at p = 0.08) [5]. *Jensen et al.* also observed higher LC rates after five years for the combined RT group in a comparable study (60% vs. 40%, p = 0.03) [4].

As far as has been published, the planning process for this type of combined RT involves unimodal treatment simulations in different therapy planning systems (TPS). A subset of the aforementioned studies evaluated cumulative dose distributions at the end of the planning stage via an RBE (Relative Biological Effectiveness) model for approximate photon-equivalent doses of the carbon irradiation. Nonetheless, there were no intermittent calculations during the iterative optimization process itself. In such separated planning strategies, insufficiencies in the cumulative dose distribution can only be acted upon by re-planning at least one modality, a time-consuming task that may require multiple repetitions. An alternative integrated planning strategy, which would include continuous dose summations already during the optimization stage of the subsequently planned modality (bias dose planning), could potentially improve upon this workflow.

Current research on combination planning is generally focused on simultaneous optimization (hybrid optimization): *Popple et al.* demonstrated this technique for a photon-only setup of sequential IMRT [6], while *Krämer et al.* used a particle-only setup of carbon and proton beams [7]. *Gao* as well as *Unkelbach et al.* published works on simultaneous optimization for proton–photon [8,9], *Mueller et al.* for electron-photon [10], and *Kueng et al.* for proton–photon-electron treatments [11]. Given that bias dose planning is an existing feature of certain commercial TPS, its clinical implementation would not require extensive software engineering. Yet it has the ability to resolve specific shortcomings in current carbon-photon planning, especially the inconvenient handling of OAR tolerance doses across both plans, until simultaneous optimization becomes clinically feasible in the future. The goal of this study was therefore to assess an integrated strategy based on bias dose planning as outlined above, using cases of head and neck malignancies for which separately planned carbon-photon RT had previously been performed at our facilities.

2. Materials and methods

2.1. Ethics approval and consent

This retrospective study was approved by the institutional review board and conducted in accordance with the Declaration of Helsinki. The need for written informed consent was waived.

2.2. Patient cohort

We selected ten patients with malignancies of the head and neck region who underwent consecutive carbon-photon RT at our institution between November 2011 and September 2012, and who we considered a representative patient population. The male to female ratio was 7:3. Mean age at the time of RT was 51 years (range: 29–74 years). All cases were primary tumors, comprising eight adenocarcinomas of the orbital, sinonasal, palate, and parotid regions, four of which were adenoid cystic carcinomas (ACC), as well as one undifferentiated malignant orbital salivary gland tumor and one sinonasal mucosal melanoma. The predominant treatment setting was adjuvant RT, complemented by one case of definitive RT. All patients underwent computed tomography (CT) with native and contrast-enhanced series for treatment planning. Individually fitted thermoplastic head masks with shoulder fixation were used for immobilization. Additional information on the patient cohort is compiled in Supplementary Table S1.

2.3. Planning and setup details for carbon IBT

IBT treatments were inversely planned in Syngo RT Planning (VB10A and VB10B, Siemens AG, Germany). Field configurations varied between one to four horizontal C12 beams positioned at different angles to deliver carbon ions via the active raster-scanning technique. Optimization modes included intensity-modulated particle therapy and single beam optimization. The first iteration of the Local Effect Model (LEM 1) was used for RBE calculation and carbon doses subsequently quantified in GyE (Gray Equivalents). The clinical target volume (CTVboost) involved the macroscopic tumor and/or tumor bed (median volume: 153 cm^3, range: 60–245 cm^3), and was complemented by a planning target volume (PTV) with an isotropic margin of 3 mm. Median doses to CTVboost were normalized to deliver 24 GyE in 8 fractions of 3 GyE, while aiming for coverage by the 95% isodose line. Image guidance was performed via daily orthogonal x-ray images.

2.4. Planning and setup details for photon IMRT

The clinical IMRT treatments were inversely planned in TomoTherapy PlanningStation (4.0.3.28 to 4.2.0.87, Accuray, USA) for helical tomotherapy (HT-IMRT) using a TomoHD treatment machine. The structure sets from the previously planned IBT were reutilized. Beam energies were set to 6 MV and longitudinal field widths defined in the range of 1.0–2.5 cm, with a uniform pitch of 0.43. Intensity modulation factors were planned in the range of 2.4–2.8, resulting in actual factors of 1.57 to 2.33. The clinical target volume (CTVelective) included CTVboost as well as local growth patterns (median volume: 303 cm^3, range: 106–459 cm^3), again supplemented by an isotropic 3 mm PTV expansion. Plans were normalized to deliver a median dose of 50 Gray (Gy) to CTVelective in 25 fractions of 2 Gy, aiming for coverage by the 90% isodose line. OAR maximum doses were manually summated from carbon IBT and photon IMRT to ensure that even in a "worst-case scenario" of spatially coinciding maxima, no tolerance thresholds would be violated.

In our experimental integrated planning strategy, we employed RayStation (4.0.3.4 to 4.5.0.19; RaySearch Laboratories, Sweden) calibrated to an Artiste treatment machine (Siemens AG, Germany) for inverse planning of step-and-shoot IMRT (segmental multileaf collimation IMRT; SMLC-IMRT). The effective carbon dose distributions were imported into RayStation following limited metadata modification, and specified as "background doses" (bias doses) for the new SMLC-IMRT plans, allowing for beam positioning and dose optimization in consideration of the carbon dose matrix. A coplanar nine-beam star shot configuration with beam energies of 6 MV and a maximum of 150 segments was chosen consistently for all treatment plans. Replicating the originally prescribed doses, the SMLC-IMRT plans were normalized to median cumulative doses of 74 GyE to CTVboost and 50 GyE to the exclusive volume of CTVelective (Fig. 1). The planning process was not blinded to the dose/volume parameters of the clinical combination plans, which were also imported into the TPS, to allow addressing of previous weak spots. RayStation utilizes three-dimensional collapsed cone convolution algorithms to compute final dose distributions, as does TomoTherapy PlanningStation. Image guidance was performed via daily megavoltage cone beam CT in both IMRT settings.

2.5. Comparison of cumulative dose distributions

A selection of dosimetric parameters was read from the cumulative dose distributions originating from both planning approaches via the scripting interface of RayStation (Supplementary Table S2). Additional derived metrics included integral doses to subject volumes (ID), as well as homogeneity and conformity indices for target volumes (HI and CI, for metric definitions see Supplementary material). ID assessment was omitted in one instance due to an additional CTV in the original plans
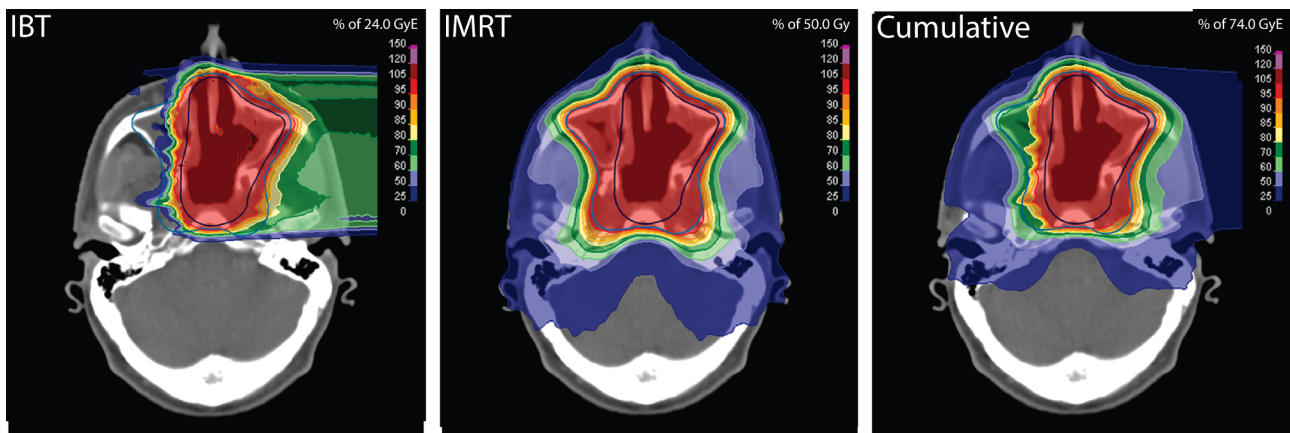
Fig. 1. The final dose distributions of carbon IBT and photon IMRT were added to obtain cumulative bimodal dose distributions (using the LEM for photon-equivalent dose calculation). *Images show identical axial planes.* (For interpretation of the references to colour in this figure legend, the reader is referred to the web version of this article.)

targeting the lymphatic pathways (case #10). OARs were partially excluded in a subset of cases due to tumor infiltration or following surgical resection. Paired OARs were categorized as contralateral if greater than or equal to two thirds of the two clinical target volumes were located on the opposite side; otherwise, both organs were designated ipsilateral. Statistical testing was conducted in MATLAB (9.2; Math-Works, USA), using a two-sided Wilcoxon matched-pair signed-rank test with a significance threshold of $\alpha = 0.05$.

For a case-by-case comparison oriented towards radiobiological risk, additional cumulative dose distributions were calculated based on equivalent doses at 2 Gy(E) per fraction (EQD2) [12]. This was accomplished through an in-house software, which applied the linear-quadratic model (LQM) to each dose bin D_i of the carbon dose distributions according to the equation

$$EQD_i 2 = D_i \frac{\frac{D_i}{n} + \frac{\alpha}{\beta}}{2GyE + \frac{\alpha}{\beta}}$$

thus yielding the desired isoeffective carbon dose distributions in 2 GyE fractions (where n is the number of fractions and α/β is assumed to be 3). Threshold values for toxicity risks were adopted from organ-specific QUANTEC papers and *Emami et al.* [13] for 1.8–2.0 Gy per daily fraction, with units changed to GyE without further adjustment, and evaluated as $D_{1\%}$ (Supplementary Table S3). The retina was assessed as the posterior segment of the eyeball rather than delineated separately.

3. Results

3.1. Target volumes

The median DVH plots showed that for the integrated planning strategy, both the CTVboost and the CTVelective curves had moved slightly further towards their respective prescription isodoses of 74 GyE and 50 GyE (Fig. 2a). These differences also became evident in the majority of conformity and homogeneity indices: CI_{boost} (median 0.95 for the integrated strategy vs. 0.87 for the separated strategy, p = 0.002, Fig. 3 shows a case example) as well as HI_{boost} (median 0.94 vs. 0.93, p = 0.03) and $HI_{elective}$ (median 0.68 vs. 0.66, p = 0.047) demonstrated statistically significant gains, meanwhile $CI_{elective}$ did not achieve statistical significance (median 0.34 vs. 0.30, p = 0.2). Coverages presented statistically significant differences only for CTVelective, as was evident from a moderate increase in $Cov_{95\%}$ (median 98.8 vs. 98.3, p = 0.002). For additional results cf. Table 1.

3.2. Organs at risk and integral doses

Structures of the CNS showed statistically significant reductions in all median, mean and maximum dose parameters gathered for evaluation. The largest decreases involved the cranial aspect of the spinal cord (median −37%, p = 0.002 for D_{mean}, Fig. 2f), as well as the contralateral temporal lobe (median −35%, p = 0.03 for D_{mean}, Fig. 2d). Of the ten instances where EQD2-adjusted $D_{1\%}$ to the ipsilateral temporal lobe ranged above the toxicity risk threshold of 60 GyE in the clinical plans, two instances were moved below this value in the experimental plans (cases #1 and #8, Fig. 4).

Structures of the optical system (strictly speaking also belonging to the CNS) demonstrated statistically significant overall reductions in all median and mean dose values. Notably relevant in the context of their serial architecture, the optic nerves experienced lower near-maximum doses $D_{1\%}$ when employing the integrated strategy (median −2%, p = 0.03 for ipsilateral and −25%, p = 0.03 for contralateral, Fig. 2gh). Maximum dose $D_{1\%}$ to the optic chiasm did not show statistical significance (Fig. 2i). Of the seven instances where EQD2-adjusted $D_{1\%}$ to the ipsilateral retina ranged above the threshold of 50 GyE in the clinical plans, two instances were moved below this level in the experimental plans (cases #5 and #8), as was the one instance where $D_{1\%}$ to the ipsilateral optical nerve previously crossed the threshold of 55 GyE (case #6, Fig. 4).

The parotid glands profited from the integrated planning strategy in the evaluation of D_{mean} (median −14%, p = 0.001 for ipsilateral and −25%, p = 0.03 for contralateral, Supplementary Fig. S1). EQD2-adjusted bilateral mean dose was reduced in all instances; in the one instance where the clinical plan exceeded the threshold of 25 GyE for an elevated risk of grade 4 xerostomia, the integrated planning strategy yielded a reduced dose of 18 GyE (case #10, Fig. 4).

Decreases in integral dose were observed in seven instances (median −37%). For the remaining two instances, the integrated strategy resulted in increases of +16% and +2% (cases #01 and #06). Overall, the changes did not achieve statistical significance (median −12% for n = 9, p = 0.07). For additional results cf. Table 2.

4. Discussion

In this paper, we presented comparative data on plan quality for carbon-photon RT, generated using two distinct planning approaches with different levels of inter-modality dependence. To our knowledge, this is the first study to investigate carbon-photon bias dose planning in this manner. The results showed statistically significant differences for target irradiation and normal tissue sparing, which were predominantly in favor of the closer integrated approach.
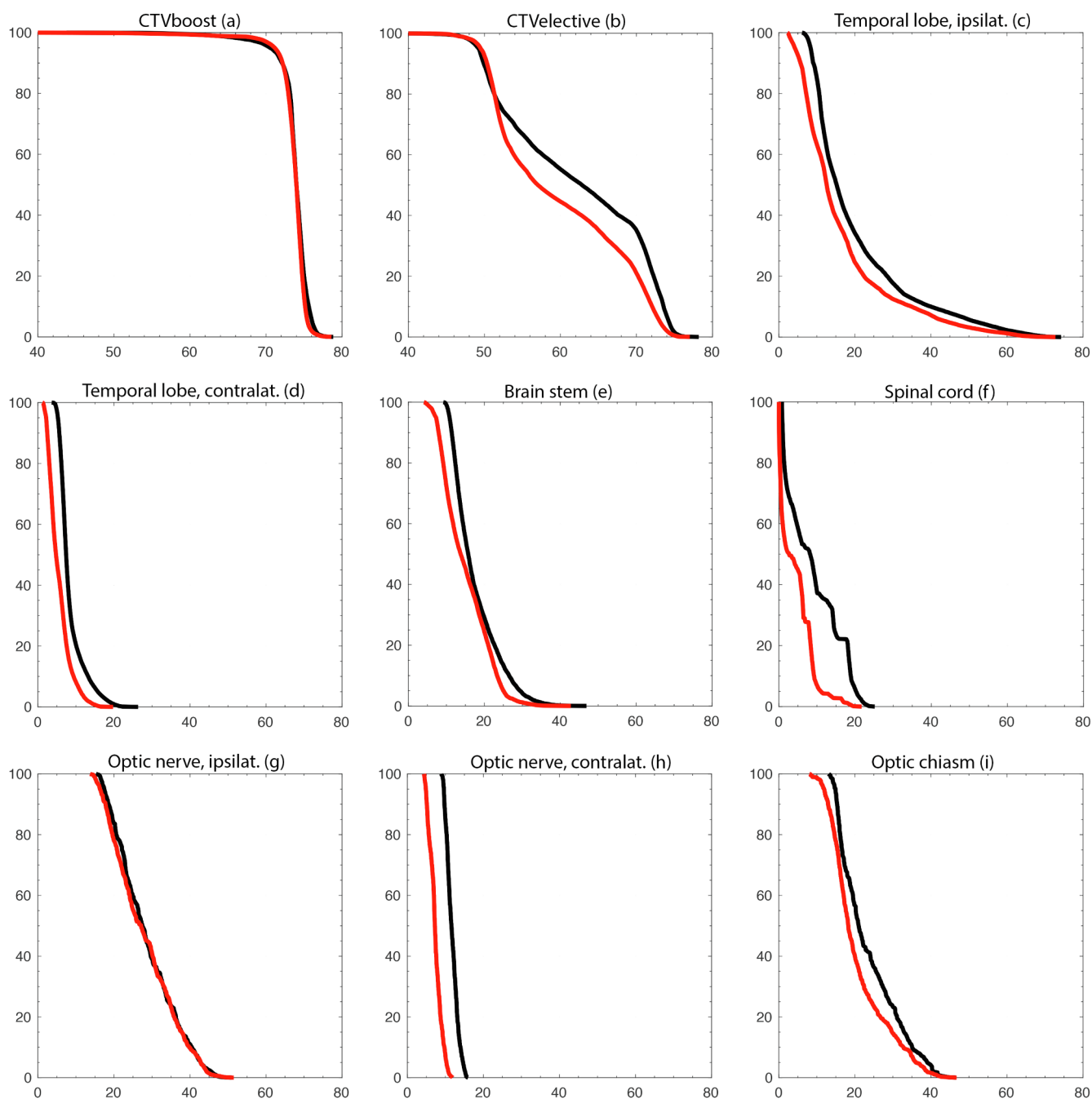
Fig. 2. Cumulative dose-volume histograms for carbon-photon RT. Median data of the patient cohort (n = 10) was used for both clinical target volumes and OARs. *The abscissa displays the volume in %. The ordinate displays the dose in GyE. Black marks the clinical separated planning strategy. Red marks the experimental integrated planning strategy.* (For interpretation of the references to colour in this figure legend, the reader is referred to the web version of this article.)

Previously published studies on carbon-photon RT already achieved positive results over other treatment forms, with respect to plan quality as well as clinical outcomes, via independent planning of both modalities (in some instances complemented by the evaluation of cumulative dose distributions as verification) [2–5]. For our study, we decided to optimize the photon plans on top of the carbon plans. A reverse approach could have exploited the versatility and high precision of heavy ion delivery for adapting to a background dose, yet, when this study was conducted, a TPS with this capability was not commercially available. However, given that carbon IBT with active raster scanning achieves exceptional homogeneity of target dose deposition, our subsequent planning of photon IMRT did not have to flexibly compensate for preexisting inhomogeneities in target regions.

Our results confirm that the cumulative dose distributions did benefit from the integrated planning approach, mainly by improved conformity to the boost volume as well as organ sparing. This is in addition to the streamlined and cost-effective workflow that an integrated planning strategy provides. These observations can in part be analogized to those made recently in the comparison of sequential and simultaneous integrated boost techniques in IMRT [14]. Further research as well as clinical application will be assisted by a new generation of TPS with built-in support for combination planning of carbon-photon RT, as this will obviate the need for data modification. Finally, the highest level of integration will be achieved in the form of simultaneous optimization. This technique has already been effectively demonstrated for a variety of modality combinations as laid out in the
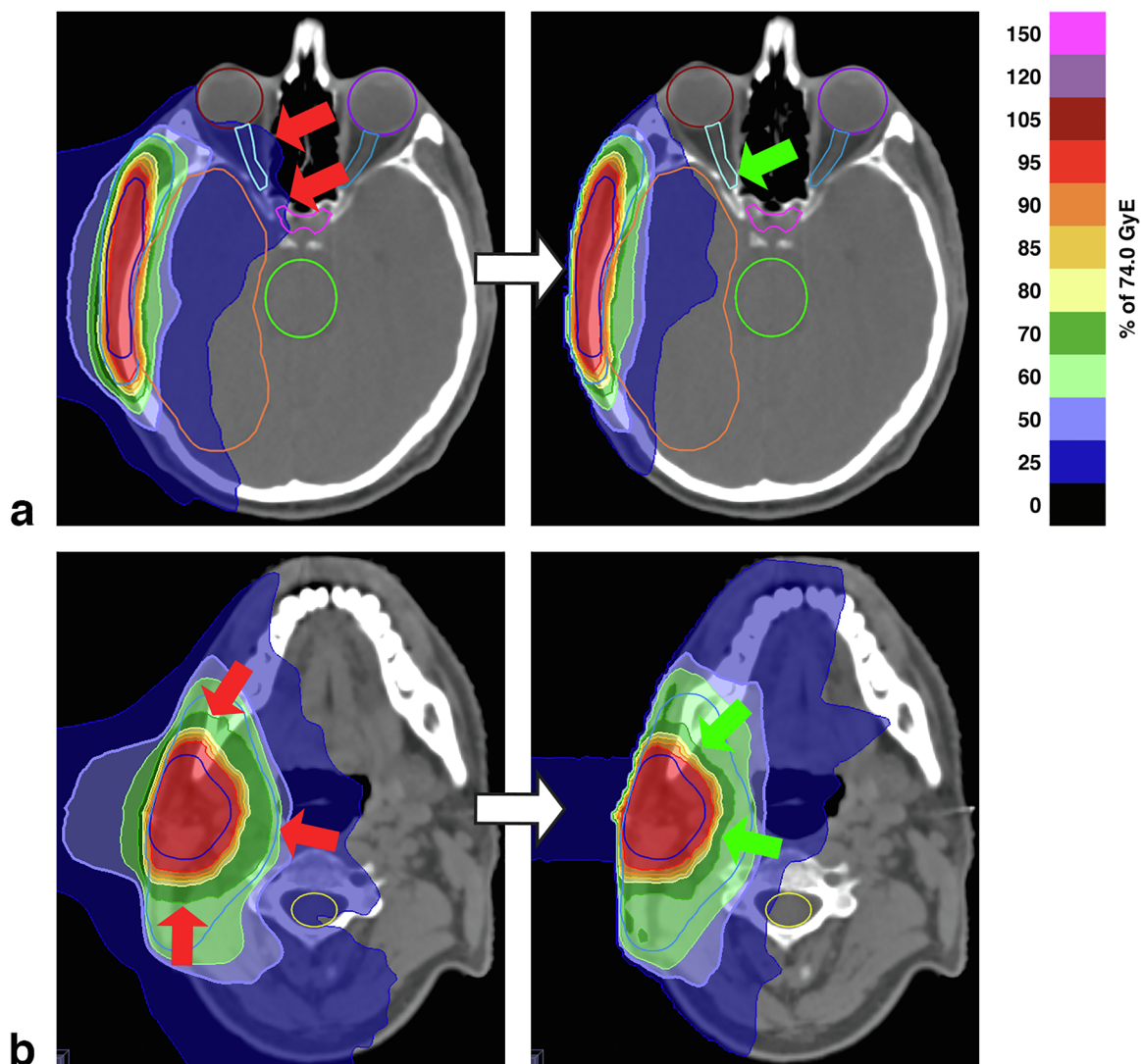
Fig. 3. Case example of an adenoid adenocarcinoma in the right parotid gland (case #07). The target volumes measured 245 cm³ for CTVboost and 459/220 cm³ for CTVelective (inclusive/exclusive volumes). The integrated planning strategy resulted in improved sparing of the right visual pathway (a) and the right temporal lobe (b). The conformities of the 74 and 50 GyE isodoses to the target volumes were maintained and, in some areas, improved (CI$_{boost}$ 0.95 for the integrated strategy vs. 0.90 for the separated strategy, CI$_{elective}$ 0.38 vs. 0.39). *Images from cranial to caudal. Arrows indicate adverse (red) and favorable (green) dose distribution characteristics.* (For interpretation of the references to colour in this figure legend, the reader is referred to the web version of this article.)

Table 1
Results for CTVs: Parameters of the cumulative dose distributions that emerged from the separated and the integrated planning strategy. *Values for CTVelective are based on exclusive volumes. Bold denotes statistical significance at level p < 0.05.*

Volume (n)	Parameter	Separated Strategy Median (IQR)		Integrated Strategy Median (IQR)		ΔMedian (%)		p
CTVboost (10)	$D_{99\%}$	63.2	(10.2)	63.6	(12.0)	+ 0.3	(+ 1%)	0.1
	$D_{98\%}$	66.9	(7.9)	69.1	(7.4)	+ 2.2	(+ 3%)	**0.006**
	$D_{50\%}$	74.0	(0.3)	74.0	(0.1)	± 0.0		0.5
	$D_{2\%}$	76.5	(0.8)	76.0	(0.5)	− 0.6	(− 1%)	**0.004**
	$D_{1\%}$	76.8	(0.7)	76.5	(0.7)	− 0.4	(± 0%)	**0.004**
	$Cov_{100\%}$	50.2	(10.4)	50.2	(2.7)	± 0.0		0.9
	$Cov_{95\%}$	95.8	(4.6)	96.8	(5.1)	+ 1.0	(+ 1%)	0.6
	CI_{boost}	0.87	(0.07)	0.95	(0.04)	+ 0.08	(+ 9%)	**0.002**
	HI_{boost}	0.93	(0.03)	0.94	(0.04)	+ 0.01	(+ 1%)	**0.03**
CTVelective (10)	$D_{99\%}$	46.2	(1.5)	46.9	(1.6)	+ 0.7	(+ 2%)	**0.002**
	$D_{98\%}$	47.8	(2.0)	48.3	(1.5)	+ 0.6	(+ 1%)	**0.04**
	$D_{50\%}$	64.0	(8.0)	57.1	(5.0)	− 6.9	(− 11%)	**0.01**
	$D_{2\%}$	74.8	(0.6)	74.0	(0.6)	− 0.9	(− 1%)	**0.002**
	$D_{1\%}$	75.3	(0.6)	74.5	(0.5)	− 0.8	(− 1%)	**0.002**
	$Cov_{100\%}$	89.8	(11.6)	92.7	(6.9)	+ 3.0	(+ 3%)	0.2
	$Cov_{95\%}$	98.3	(1.6)	98.8	(1.8)	+ 0.5	(+ 1%)	**0.002**
	$CI_{elective}$	0.30	(0.12)	0.34	(0.10)	+ 0.02	(+ 3%)	0.2
	$HI_{elective}$	0.66	(0.02)	0.68	(0.03)	+ 0.04	(+ 14%)	**0.047**
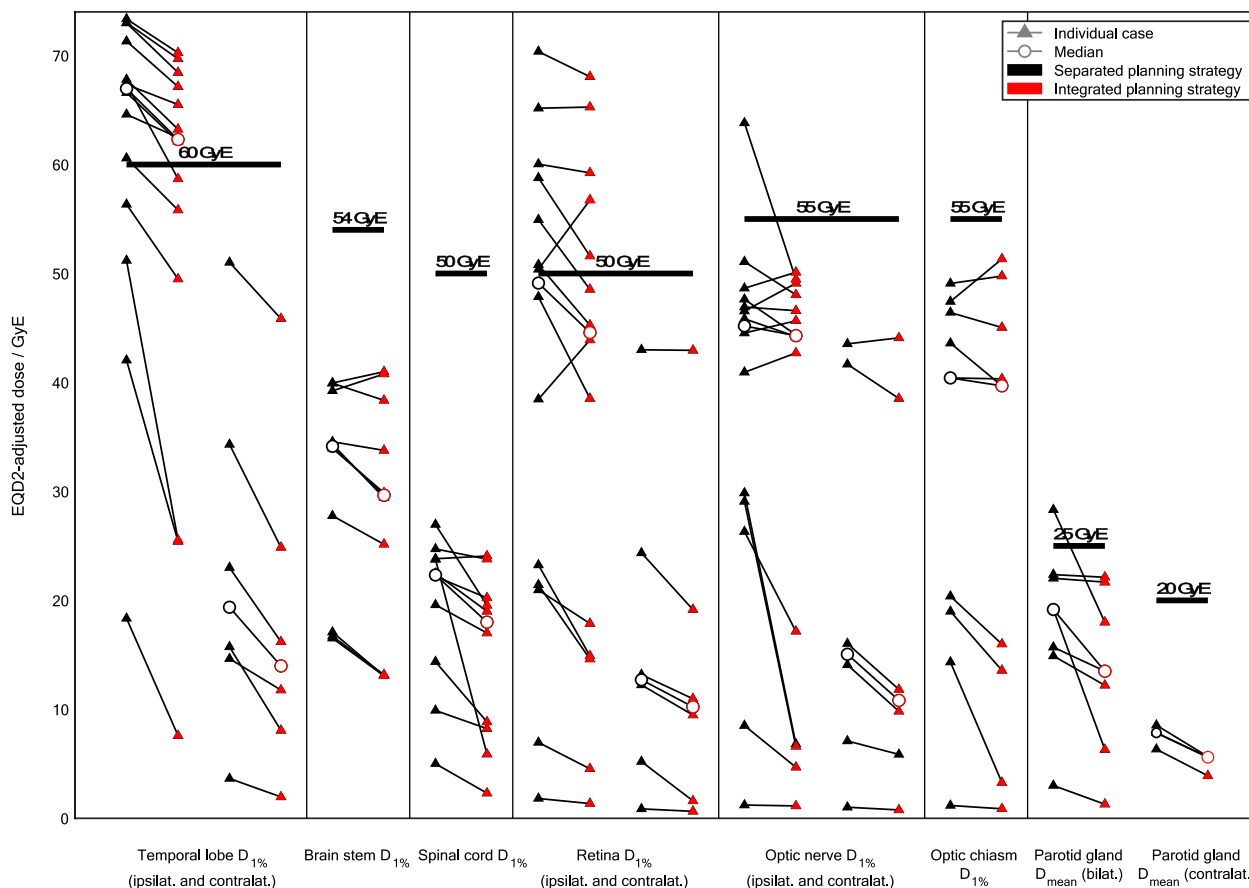
Fig. 4. A case-by-case comparison between both planning strategies, oriented towards radiobiological risk. Individual values are based on EQD2-adjusted cumulative dose distributions (with an α-β-ratio of 3). Threshold values and their clinical endpoints are listed in Supplementary Table S3.

introduction, and it will most likely be realized for carbon-photon planning as well in the near future. Inferring from the aforementioned studies, notably those by *Gao* as well as *Unkelbach et al.* for proton–photon combinations of intensity-modulated proton therapy (IMPT) and IMRT [8,9], this holds potential of further improvements in plan quality.

In this study, we used the LEM for predicting the RBE value of a high-LET (linear energy transfer) heavy ion radiation. The authors of the model argue that within the center of the charged particle track, i.e., on a *local* nanometer level, the spatial dose distribution becomes homogenous and may be approximated to that of a low-LET photon radiation [15]. Other RBE models have also been postulated, such as

Table 2
Results for OARs: Parameters of the cumulative dose distributions that emerged from the separated and the integrated planning strategy. *Bold denotes statistical significance at level p $<$ 0.05.*

Volume (n)	Parameter	Separated Strategy Median (IQR)		Integrated Strategy Median (IQR)		ΔMedian (%)		p
Temporal lobe	D_{mean}	20.4	(3.1)	17.1	(2.2)	−3.3	(−16%)	**< 0.001**
ipsilat. (14)	$D_{1\%}$	65.4	(8.8)	60.9	(12.5)	−4.5	(−7%)	**< 0.001**
Temporal lobe	D_{mean}	8.4	(7.4)	5.5	(6.1)	−2.9	(−35%)	**0.03**
contralat. (6)	$D_{1\%}$	19.9	(17.6)	14.4	(14.3)	−5.5	(−28%)	**0.03**
Brainstem (10)	$D_{50\%}$	15.8	(8.4)	13.8	(12.4)	−2.0	(−13%)	**0.002**
	$D_{1\%}$	35.3	(18.7)	30.4	(21.9)	−4.9	(−14%)	**0.01**
Spinal cord (10)	D_{mean}	8.1	(5.1)	5.1	(5.4)	−3.0	(−37%)	**0.002**
	$D_{1\%}$	22.5	(7.7)	18.2	(11.4)	−4.2	(−19%)	**0.004**
Posterior eyeball	D_{mean}	23.9	(20.3)	20.2	(20.8)	−3.6	(−15%)	**0.005**
ipsilat. (14)	$D_{1\%}$	49.8	(35.8)	44.9	(40.0)	−4.8	(−10%)	0.06
Posterior eyeball	D_{mean}	6.8	(8.4)	5.1	(5.9)	−1.7	(−25%)	**0.03**
contralat. (6)	$D_{1\%}$	12.9	(15.6)	10.3	(14.0)	−2.6	(−20%)	**0.03**
Optic nerve	$D_{50\%}$	28.3	(24.4)	26.2	(23.5)	−2.1	(−8%)	**< 0.001**
ipsilat. (14)	$D_{1\%}$	46.5	(23.3)	45.8	(38.1)	−0.7	(−2%)	**0.03**
Optic nerve	$D_{50\%}$	11.5	(17.2)	7.3	(14.5)	−4.3	(−37%)	**0.03**
contralat. (6)	$D_{1\%}$	14.9	(29.3)	11.2	(25.8)	−3.7	(−25%)	**0.03**
Optic chiasm (9)	$D_{50\%}$	21.0	(19.5)	18.3	(16.0)	−2.8	(−13%)	**0.01**
	$D_{1\%}$	42.0	(28.7)	41.5	(32.6)	−0.5	(−1%)	0.055
Parotid gland ipsilat. (11)	D_{mean}	23.8	(5.8)	20.5	(11.1)	−3.3	(−14%)	**0.001**
Parotid gland contralat. (6)	D_{mean}	6.7	(1.3)	5.1	(1.4)	−1.7	(−25%)	**0.03**
Subject volume (9)	ID	61.0	(19.2)	53.4	(27.7)	−7.6	(−12%)	0.07

the Microdosimetric Kinetic Model [16]. Among the diverse benefits of these radiobiological models is that their application facilitates the conceptualization and management of a combined RT regimen with elements from both LET domains. Although the conceptual basis of the LEM has been criticized [17,18], its usage – and, by extension, the formulation of a cumulative bimodal dose – conforms to the routine clinical workflow established at our institution, which this study aims to reproduce, and is therefore used analogously. This reasoning also extends to the comparison of toxicity risks, in which we referenced dose threshold values that were originally determined on the basis of low-LET photon radiation; a practice that is still under debate and not of general validity.

The experimental IMRT plans were based on the SMLC technique, while the clinical IMRT plans belonged to an HT setup. This represents a conceptual weakness of our study, which was conducted before a TPS with support for combination planning including HT-IMRT was made available. *Chen et al.* found statistically significant advantages in conformity, homogeneity, and normal tissue sparing for HT-IMRT over a nine-beam star shot SMLC-IMRT in the treatment of nasopharyngeal carcinomas [19]. *Van Vulpen et al.* observed similar differences in their study on oropharyngeal carcinomas, although they did question the clinical relevance of the primarily minor performance gains, as did *Chen et al.* in another study on head and neck cancers [20,21]. These publications attest to a potential (dosimetric) superiority of HT-IRMT over SMLC-IMRT, and suggest that the positive results of our planning strategy are most likely not attributable to the use of a different IMRT setup. *Jensen et al.* also used both techniques interchangeably in studies on carbon-photon RT [22,23].

While not reaching statistical significance in this study, the proposed planning strategy showed potential to lessen integral doses, thereby potentiating a previously observed feature of combined carbon IBT and photon IMRT, when compared against a unimodal IMRT [24]. The risk of secondary malignancies had already been estimated in the 1980s to reach up to 23% for an eight-year period after RT of the neck region [25]. Although certainly reduced with current technologies, normal tissue radiation exposure remains relevant, especially in the context of increased life expectancies.

In conclusion, our findings indicate that combination planning of carbon-photon RT via a bias dose method may translate into favorable dose distribution characteristics, compared to independent optimization of the two modalities, in the treatment of head and neck malignancies. Additionally, our method streamlined the planning workflow by anticipating potential plan revisions. As they originate from a proof-of-principle study, the observed dosimetric improvements are yet theoretical. It remains the subject of follow-up studies, whether or not they can be validated in an in-depth review of robustness and contribute to a higher tumor control.

Declaration of Competing Interest

The authors declare that they have no known competing financial interests or personal relationships that could have appeared to influence the work reported in this paper.

Appendix A. Supplementary data

Supplementary data to this article can be found online at https://doi.org/10.1016/j.phro.2020.06.008.

References

[1] Bray F, Ferlay J, Soerjomataram I, Siegel RL, Torre LA, Jemal A. Global cancer statistics 2018: GLOBOCAN estimates of incidence and mortality worldwide for 36 cancers in 185 countries. CA Cancer J Clin 2018;68:394–424. https://doi.org/10.3322/caac.21492.

[2] Adeberg S, Akbaba S, Lang K, Held T, Verma V, Nikoghosyan A, et al. The phase 1/2 ACCEPT trial: concurrent cetuximab and intensity modulated radiation therapy with carbon ion boost for adenoid cystic carcinoma of the head and neck. Int J Radiat Oncol Biol Phys 2020;106:167–73. https://doi.org/10.1016/j.ijrobp.2019.09.036.

[3] Akbaba S, Mock A, Hoerner-Rieber J, Held T, Katayama S, Forster T, et al. Treatment outcome of a combined dose-escalated treatment regime with helical tomotherapy(R) and active raster-scanning carbon ion boost for adenocarcinomas of the head and neck. Front Oncol 2019;9:755. https://doi.org/10.3389/fonc.2019.00755.

[4] Jensen AD, Nikoghosyan AV, Poulakis M, Hoss A, Haberer T, Jakel O, et al. Combined intensity-modulated radiotherapy plus raster-scanned carbon ion boost for advanced adenoid cystic carcinoma of the head and neck results in superior locoregional control and overall survival. Cancer 2015;121:3001–9. https://doi.org/10.1002/cncr.29443.

[5] Schulz-Ertner D, Nikoghosyan A, Didinger B, Munter M, Jakel O, Karger CP, et al. Therapy strategies for locally advanced adenoid cystic carcinomas using modern radiation therapy techniques. Cancer 2005;104:338–44. https://doi.org/10.1002/cncr.21158.

[6] Popple RA, Prellop PB, Spencer SA, De Los Santos JF, Duan J, Fiveash JB, et al. Simultaneous optimization of sequential IMRT plans. Med Phys 2005;32:3257–66. https://doi.org/10.1118/1.2064849.

[7] Krämer M, Scifoni E, Schmitz F, Sokol O, Durante M. Overview of recent advances in treatment planning for ion beam radiotherapy. Eur Phys J D 2014;68. https://doi.org/10.1140/epjd/e2014-40843-x.

[8] Gao H. Hybrid proton-photon inverse optimization with uniformity-regularized proton and photon target dose. Phys Med Biol 2019;64:105003https://doi.org/10.1088/1361-6560/ab18c7.

[9] Unkelbach J, Bangert M, De Amorim BK, Andratschke N, Guckenberger M. Optimization of combined proton-photon treatments. Radiother Oncol 2018;128:133–8. https://doi.org/10.1016/j.radonc.2017.12.031.

[10] Mueller S, Fix MK, Joosten A, Henzen D, Frei D, Volken W, et al. Simultaneous optimization of photons and electrons for mixed beam radiotherapy. Phys Med Biol 2017;62:5840–60. https://doi.org/10.1088/1361-6560/aa70c5.

[11] Kueng R, Mueller S, Loebner HA, Frei D, Volken W, Aebersold DM, et al. TriB-RT: simultaneous optimization of photon, electron and proton beams. Phys Med Biol 2020. https://doi.org/10.1088/1361-6560/ab936f.

[12] Allen Li X, Alber M, Deasy JO, Jackson A, Ken Jee KW, Marks LB, et al. The use and QA of biologically related models for treatment planning: short report of the TG-166 of the therapy physics committee of the AAPM. Med Phys 2012;39:1386–409. https://doi.org/10.1118/1.3685447.

[13] Emami B. Tolerance of normal tissue to therapeutic radiation. Rep Radiother Oncol 2013:1.

[14] Dogan N, King S, Emami B, Mohideen N, Mirkovic N, Leybovich LB, et al. Assessment of different IMRT boost delivery methods on target coverage and normal-tissue sparing. Int J Radiat Oncol Biol Phys 2003;57:1480–91. https://doi.org/10.1016/S0360-3016(03)01569-4.

[15] Scholz M, Kraft G. A parameter-free track structure model for heavy ion action cross sections. In: Chadwick KH, Moschini G, Varma MN, editors. Biophysical modelling of radiation effects. Bristol, UK: Adam Hilger; 1992, p. 185–92.

[16] Hawkins RB. A microdosimetric-kinetic model of cell death from exposure to ionizing radiation of any LET, with experimental and clinical applications. Int J Radiat Biol 1996;69:739–55. https://doi.org/10.1080/095530096145481.

[17] Beuve M. Formalization and theoretical analysis of the local effect model. Radiat Res 2009;172:394–402. https://doi.org/10.1667/rr1544.1.

[18] Katz R. The parameter-free track structure model of scholz and kraft for heavy-ion cross sections. Radiat Res 2003;160:724–8. https://doi.org/10.1667/RR3088.

[19] Chen A, Lee N, Yang C, Liu T, Narayan S, Vijayakumar S, et al. Comparison of intensity-modulated radiotherapy using helical tomotherapy and segmental multi-leaf collimator-based techniques for nasopharyngeal carcinoma: dosimetric analysis incorporating quality assurance guidelines from RTOG 0225. Technol Cancer Res Treat 2010;9:291–8. https://doi.org/10.1177/153303461000900308.

[20] van Vulpen M, Field C, Raaijmakers CP, Parliament MB, Terhaard CH, MacKenzie MA, et al. Comparing step-and-shoot IMRT with dynamic helical tomotherapy IMRT plans for head-and-neck cancer. Int J Radiat Oncol Biol Phys. 2005;62:1535–9. https://doi.org/10.1016/j.ijrobp.2005.04.011.

[21] Chen AM, Marsano J, Perks J, Farwell G, Luu Q, Donald PJ, et al. Comparison of IMRT techniques in the radiotherapeutic management of head and neck cancer: is tomotherapy "better" than step-and-shoot IMRT? Technol Cancer Res Treat 2011;10:171–7. https://doi.org/10.7785/tcrt.2012.500192.

[22] Jensen AD, Nikoghosyan A, Windemuth-Kieselbach C, Debus J, Munter MW. Combined treatment of malignant salivary gland tumours with intensity-modulated radiation therapy (IMRT) and carbon ions: COSMIC. BMC Cancer 2010;10:546. https://doi.org/10.1186/1471-2407-10-546.

[23] Jensen AD, Nikoghosyan AV, Windemuth-Kieselbach C, Debus J, Munter MW. Treatment of malignant sinonasal tumours with intensity-modulated radiotherapy (IMRT) and carbon ion boost (C12). BMC Cancer 2011;11:190. https://doi.org/10.1186/1471-2407-11-190.

[24] Schulz-Ertner D, Nikoghosyan A, Didinger B, Karger CP, Jkel O, Wannenmacher M, et al. Treatment planning intercomparison for spinal chordomas using intensity-modulated photon radiation therapy (IMRT) and carbon ions. Phys Med Biol 2003;48:2617–31. https://doi.org/10.1088/0031-9155/48/16/304.

[25] Cooper JS, Pajak TF, Rubin P, Tupchong L, Brady LW, Leibel SA, et al. Second malignancies in patients who have head and neck cancer: Incidence, effect on survival and implications based on the RTOG experience. Int J Radiat Oncol Biol Phys 1989;17:449–56. https://doi.org/10.1016/0360-3016(89)90094-1.